AIAA JOURNAL
Vol. 46, No. 12, December 2008

Acoustic Diffraction by a Finite Airfoil in Uniform Flow

Wonju Jeon*
National Institute for Mathematical Sciences, Daejeon 305-340, Republic of Korea
and
Duck-Joo Lee†
Korea Advanced Institute of Science and Technology, Daejeon 305-701, Republic of Korea

DOI: 10.2514/1.32424

Diffraction by a flat airfoil in uniform flow is analytically examined, focusing on the acquisition of an accurate series solution for both low- and high-frequency incident waves. Formulation of integral equations is based on the use of the Wiener–Hopf technique in the complex domain. As the kernels of the integral equations are multivalued functions having a branch cut in the complex domain, the unknown in the integral operator is assumed to be a constant. Therefore, the solution is a zeroth-order approximate solution adequate for a high-frequency problem. In this study, the unknown is expanded by a Taylor series of an arbitrary order in the analytic region, and the solution is obtained in series form involving a special function called a generalized gamma function $\Gamma_m(u, z)$. As the generalized gamma functions occurring in finite diffraction theory have the specific argument u as "nonnegative integer $+\frac{1}{2}$," the authors used their previously determined exact and closed-form formulas of this special function to obtain the complete series solution. The present series solution exhibits faster convergence at a high frequency compared to a low frequency, whereas the Mathieu series solution in the elliptic coordinates converges faster at a low frequency relative to a higher frequency. Through exact and asymptotic evaluations of inverse Fourier transforms, the scattered and total acoustic fields are visualized in a physical domain and each term of the solution is physically interpreted as 1) semi-infinite leading-edge scattering, 2) trailing-edge correction, and 3) interaction between leading and trailing edges, respectively.

Nomenclature

a	=	speed of propagation in convected medium
c	=	speed of sound in medium at rest
F_+	=	plus functions which are analytic in the upper-half plane of the complex domain, i.e., $\mathrm{Im}(\lambda) > -\kappa_2 \cos\theta_e$
F_-	=	minus functions which are analytic in the lower-half plane of the complex domain, i.e., $\mathrm{Im}(\lambda) < \kappa_2 \cos\theta_e$
k	=	wave number of an incident wave in the physical domain
l	=	half length of the flat airfoil
U, M	=	speed and Mach number of uniform flow
x, y	=	Cartesian coordinate in the physical domain
$\Gamma_m(u, z)$	=	generalized gamma function (gamma function for $m = 0$)
θ_i, θ_e	=	incidence angle in physical and the nondimensional Prandtl–Glauert domain
κ	=	wave number of an incident wave in the nondimensional Prandtl–Glauert domain ($\kappa = \kappa_1 + i\kappa_2$, $\kappa_1 \gg \kappa_2 > 0$)
λ	=	independent variable in the complex domain
ξ, η	=	Cartesian coordinate in the nondimensional Prandtl–Glauert domain
Φ	=	scattered acoustic potential in the complex domain (Fourier transform of ϕ)
φ	=	acoustic potential in the physical domain
ϕ	=	scattered acoustic potential in the nondimensional Prandtl–Glauert domain
Ψ	=	unknown function in the Wiener–Hopf integral equation

Presented as Paper 2839 at the 11th AIAA/CEAS Aeroacoustics Conference, Monterey, CA, 23–25 May 2005; received 9 June 2007; accepted for publication 11 August 2008.

*Postdoctoral Researcher, Division of Industrial Mathematics, 385-16, Doryong-dong, Yuseong-gu. Member AIAA

†Professor, Division of Aerospace Engineering, 373-1, Guseong-dong, Yuseong-gu. Member AIAA

I. Introduction

AN AIRFOIL encountering a small perturbation convected in the wind can be studied analytically by modeling the airfoil and the small perturbation by a thin/flat airfoil and a monochromatic plane wave in uniform flow, respectively, for mathematical convenience. This flat airfoil is called a finite strip, and the flow is parallel to the strip to avoid generating lift force on the strip. This problem is governed by a convective wave equation of acoustic potential, and the corresponding boundary condition is imposed *on* the strip as an impermeability condition of Neumann type. Meanwhile, because the boundary conditions *ahead of* and *behind* the strip are given as Dirichlet type, the major difficulty in mathematical analyses has been to solve this three-part mixed boundary value problem (MBVP). In this paper, the authors focus on improving the mathematical analysis of this simplified problem so that the methodology and results can be applied to similar problems in the fields of optics, electromagnetism, and acoustics.

Since the exact solution of a semi-infinite problem was obtained by Sommerfeld [1] in 1896 for optical waves, diffraction by a finite strip has seen extensive study. The first outstanding work on a finite strip was published by Schwarzschild [2] in 1902. He obtained a solution by solving iterative semi-infinite problems through modifications of unsatisfied boundary conditions. This approximate analysis is physically reasonable and is advantageous in that each semi-infinite problem has two-part mixed boundary conditions. The existing formulas for the far-field acoustics by Amiet [3] and Martinez and Widnall [4] were derived using Schwarzschild's concept [2]. However, an iterative analysis becomes highly complicated when the number of iterations is increased so as to improve accuracy, especially in the case of low-frequency incident waves. Therefore, this method usually ends with only a single iteration, which is acceptable in the case of a high-frequency problem. In terms of accuracy, the most rigorous and the only exact solution obtained to date is the Mathieu [5] series solution set forth by

Morse and Rubenstein [6] in 1938. They regarded the finite strip as a degenerate ellipse and separated the wave equation in the elliptic coordinates following the original idea of Sieger [7] in 1908. In spite of its exactness, this solution has rarely been used (recently, the Mathieu [5] series solution was used for a validation example of a silent aircraft technology [8]), due to its poor convergence in the high-frequency range and difficulties [9,10] in employing the Mathieu functions. To describe the high-frequency diffraction phenomena with reasonable accuracy, Keller [11] developed the geometrical theory of diffraction (GTD), a well-known asymptotic theory. GTD is physically comprehensive and has been widely used in acoustics, electromagnetism, and optics. However, it is not valid in the neighborhood of shadow and reflection boundaries of incident waves and also cannot be employed to analyze grazing incidence problems. Following these works, a number of attempts were made to obtain an exact solution in a convenient form for electromagnetic and acoustic waves, as reviewed by Luneburg [12] in 1996.

The major difficulty commonly manifested in the analytical considerations in these works is the geometric finiteness of the strip. As the strip is of a finite length, boundary conditions are imposed as a three-part mixed type along the strip line. Generally, a MBVP cannot be solved by conventional methods, such as those involving the separation of variables or a standard Fourier transform.

A function theoretic method called the Wiener–Hopf technique [13,14] has proven a powerful tool for MBVPs and has yielded exact solutions for certain types of geometry of two-part MBVPs. However, simultaneous integral equations inevitably appear with a multivalued kernel when the Wiener–Hopf technique is applied to a three-part MBVP, such as diffraction by a strip or a slit. As no solution technique exists for these coupled integral equations, Abrahams and Lawrie [15], Abrahams [16], and Crighton [17] have studied approximate and asymptotic factorizations of the branched Wiener–Hopf kernel. Furthermore, significant research by Latta [18], Williams [19], and Shanin [20,21] employing a novel approach that does not use the Wiener–Hopf technique has been conducted. A solution technique for the Wiener–Hopf integral equation was introduced in a book by Noble [14]. He used the simplifying technique of Jones [22], constructed two simultaneous integral equations, and then decoupled these into two single equations. Additionally, using Noble's approach [14], Kobayashi [23] analyzed electromagnetic diffraction by a strip and obtained an asymptotic solution that was superior to that of GTD. However, these works [14,23] were restricted to a zeroth-order analysis that assumed the unknown inside the integral to be a constant: they are thus valid only for high-frequency problems.

This paper provides an improved solution technique to solve the Wiener–Hopf integral equation. As the formulation procedure of the integral equations is based on the work of Noble [14] and Jones [22], in this paper, only a brief summary of the formulation of the proposed problem is given in Sec. III. In Sec. IV, the unknown inside the integral is expanded by a Taylor series of arbitrary order, and the integral terms including the unknown are analytically evaluated in the form of the generalized gamma functions of $\Gamma_m(u, z)$. The original integral equations are then recast into the simultaneous algebraic equations to determine the differential coefficients of each term in the series by solving the matrix system. However, because the generalized gamma functions are not in a closed form, but in an integral form, evaluation of the function values and their derivatives is the main difficulty when attempting to obtain a higher-order solution. As the generalized gamma function occurring in finite diffraction theory has a specific argument u as nonnegative integer $+\frac{1}{2}$, the authors used their previously formulated exact and closed-form formula [24] for this special function to obtain a complete series solution. In Sec. V, the scattered and total acoustic field and directivity patterns are visualized in the physical domain with the inclusion of fluid convection, and each term of the solution is interpreted with its physical meaning as 1) semi-infinite leading-edge scattering, 2) a trailing-edge correction, and 3) an interaction between the leading and trailing edges, respectively. The physical meaning of the second term is also heuristically explained in connection with diffraction by semi-infinite leading and trailing edges.

II. Problem Definition

A. Governing Equation

A strip of length $2l$ ($-l < x < l$, $y = 0$) encounters a small perturbation within the subsonic uniform flow U parallel to the strip, as shown in Fig. 1. The strip is assumed to be infinitesimally thin and straight, and the perturbation to the mean flow is assumed to be a time-harmonic plane wave with a time factor of $e^{-i\omega t}$. This incoming wave naturally causes the scattered velocity perturbation to have the same time factor as the incident wave.

The total acoustic potential, denoted by the subscript t, can then be described at any point by the superposition of incident and scattered potentials, denoted by the subscripts i and s, respectively:

$$\varphi_t(x, y, t) = \varphi_i(x, y, t) + \varphi_s(x, y, t) \tag{1}$$

where $\varphi_i(x, y, t) = \exp[i(kx\cos\theta_i + ky\sin\theta_i) - i\omega t]$ and $\varphi_s(x, y, t) = \varphi(x, y)e^{-i\omega t}$. Here, θ_i is the incidence angle, ω is the temporal angular frequency, and k is the incident wave number defined by ω/c, where c is the speed of sound in a stationary medium. The governing equation for the spatial acoustic potential $\varphi(x, y)$ is then written by Eq. (2), where M is the Mach number defined by U/c:

$$[(1 - M^2)\partial_x^2 + 2ikM\partial_x + \partial_y^2 + k^2]\varphi(x, y) = 0 \tag{2}$$

To alleviate the complexity due to the presence of uniform flow, the nondimensional Prandtl–Glauert (NPG) coordinates are introduced with the definitions of the acoustic potential ϕ and the wave number κ given in Eq. (3):

$$\begin{aligned} &\xi = x/l, \qquad \eta = \beta y/l, \\ &\beta = (1 - M^2)^{1/2} \quad \text{and} \quad \varphi(x, y) = \phi(\xi, \eta)e^{-i\kappa M\xi} \end{aligned} \tag{3}$$

where $\kappa = \beta^{-2}kl$. Equation (2) is then recast into the Helmholtz equation of Eq. (4):

$$(\partial_\xi^2 + \partial_\eta^2 + \kappa^2)\phi(\xi, \eta) = 0 \tag{4}$$

Here, the incident wave $\varphi_i(x, y) = \exp[ik(x\cos\theta_i + y\sin\theta_i)/(1 + M\cos\theta_i)]$ is equivalently rewritten by $\phi_i(\xi, \eta) = \exp[i\kappa(\xi\cos\theta_e + \eta\cos\theta_e)]$.

B. Boundary Conditions

The flow normal to the strip should be impermeable, so that the incident velocity perturbation will induce a scattered field that must satisfy the boundary condition, such that the normal derivative of the total acoustic potential on the strip is zero. This is written as Eq. (5a). The normal derivative of the scattered potential is continuous everywhere on $\eta = 0$, as expressed by Eq. (5b). However, the potential is continuous except for the strip region, as written in Eq. (5c). For the use of the Wiener–Hopf technique, κ is assumed to have a small positive imaginary part κ_2, that is, $\kappa = \kappa_1 + i\kappa_2$. The positive κ_2 causes the scattered potential to decay exponentially at infinity, and this behavior at infinity yields the fourth boundary condition, as expressed by Eq. (5d). After the solution is obtained, this damping factor is set to be zero:

$$\phi_\eta(\xi, 0) = -i\kappa\sin\theta_e e^{i\kappa\xi\cos\theta_e} \quad \text{on } \eta = 0 \quad \text{for } -1 < \xi < 1 \tag{5a}$$

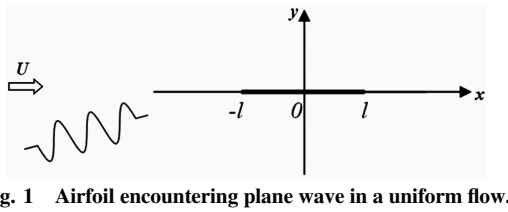

Fig. 1 Airfoil encountering plane wave in a uniform flow.

$$\phi_\eta(\xi,+0)=\phi_\eta(\xi,-0)\quad \text{for } -\infty<\xi<\infty \tag{5b}$$

$$\phi(\xi,+0)=\phi(\xi,-0)\quad \text{for } \xi<-1 \quad \text{or} \quad 1<\xi \tag{5c}$$

For any fixed η,

$$\begin{aligned}|\phi|<D_1\exp[-\kappa_2\xi\cos\theta_e]\quad \text{as } \xi\to\infty \quad \text{and}\\ |\phi|<D_2\exp[\kappa_2\xi\cos\theta_e]\quad \text{as } \xi\to-\infty\end{aligned} \tag{5d}$$

III. Formulation of the Wiener–Hopf Integral Equation

A. Wiener–Hopf Equation

The Fourier transform pairs of the unknown scattered potential ϕ are defined by Eq. (6):

$$\begin{aligned}\Phi(\lambda,\eta)&=\int_{-\infty}^{\infty}\phi(\xi,\eta)e^{i\xi\lambda}\,d\xi \quad \text{and}\\ \phi(\xi,\eta)&=(2\pi)^{-1}\int_{-\infty}^{\infty}\Phi(\lambda,\eta)e^{-i\xi\lambda}\,d\lambda\end{aligned} \tag{6}$$

From Eq. (5d), the transformed potential can be rewritten as

$$\Phi(\lambda,\eta)=e^{-i\lambda}\Phi_-(\lambda,\eta)+e^{\pm i\lambda}\Phi_\mp^0(\lambda,\eta)+e^{i\lambda}\Phi_+(\lambda,\eta) \tag{7}$$

where

$$\Phi_-(\lambda,\eta)=\int_{\infty}^{-1}\phi(\xi,\eta)e^{i(\xi+1)\lambda}\,d\xi$$

$$\Phi_\mp^0(\lambda,\eta)=\int_{-1}^{1}\phi(\xi,\eta)e^{i(\xi\mp1)\lambda}\,d\xi$$

$$\Phi_+(\lambda,\eta)=\int_{1}^{\infty}\phi(\xi,\eta)e^{i(\xi-1)\lambda}\,d\xi$$

Every "minus" function, such as Φ_-, is analytic in the lower-half complex plane of $\mathrm{Im}(\lambda)<\kappa_2\cos\theta_e$. And, every "plus" function, such as Φ_+, is analytic in the upper-half complex plane of $-k_2\cos\theta_e<\mathrm{Im}(\lambda)$, respectively.

Now, by taking the Fourier transform of Eq. (4), an ordinary differential equation is obtained as shown:

$$[\partial_\eta^2-\gamma^2(\lambda)]\Phi(\lambda,\eta)=0 \tag{8}$$

where $\gamma(\lambda)=(\lambda^2-\kappa^2)^{1/2}=\gamma_-(\lambda)\gamma_+(\lambda)$ and $\gamma_-(\lambda)=(\lambda-\kappa)^{1/2}$, $\gamma_+(\lambda)=(\lambda+\kappa)^{1/2}$. The general solution of Eq. (8) is obtained by Eq. (9) using the boundary condition Eq. (5b) and the nondiverging condition at infinity:

$$\Phi(\lambda,\eta)=\begin{cases}A(\lambda)e^{-\gamma(\lambda)\eta}, & \eta>0\\ -A(\lambda)e^{\gamma(\lambda)\eta}, & \eta<0\end{cases} \tag{9}$$

Thus, two expressions of the transformed potential Φ are given. The first is Eq. (7), as expressed by Fourier transforms of the acoustic potentials, and the second is Eq. (9), as expressed by the coefficient function $A(\lambda)$.

Setting $\eta=+0$ and $\eta=-0$ in Eq. (7) and taking the difference of the resultant equations with the use of the boundary condition given in Eq. (5c), the following equation is obtained:

$$2A(\lambda)=e^{\pm i\lambda}\Phi_\mp^0(\lambda,+0)-e^{\pm i\lambda}\Phi_\mp^0(\lambda,-0)\equiv 2e^{\pm i\lambda}\Phi_\mp^d(\lambda) \tag{10}$$

Here, Φ^d indicates the difference in the transformed potential between $\eta=+0$ and $\eta=-0$ on the finite strip.

The Fourier transform of η derivatives of Eqs. (7) and (9) are considered at this point. Differentiating by η, setting $\eta=0$, and matching the resultant equations results in

$$e^{-i\lambda}\Phi_-'(\lambda,0)+\int_{-1}^{1}\phi_\eta(\xi,0)e^{i\xi\lambda}\,d\xi+e^{i\lambda}\Phi_+'(\lambda,0)=-\gamma(\lambda)A(\lambda) \tag{11}$$

Here, both *prime* and the subscript η denote the derivatives with respect to η. The definite integral in Eq. (11) can be evaluated as shown next, using the impermeability boundary condition of Eq. (5a):

$$\begin{aligned}\int_{-1}^{1}\phi_\eta(\xi,0)e^{i\xi\lambda}\,d\xi&=-\int_{-1}^{1}i\kappa\sin\theta_e e^{i\kappa\xi\cos\theta_e}e^{i\xi\lambda}\,d\xi\\ &=-\frac{q}{\lambda+p}(e^{i(\lambda+p)}-e^{-i(\lambda+p)})\end{aligned} \tag{12}$$

where $p=\cos\theta_e$ and $q=\sin\theta_e$. Finally, combining Eqs. (10–12), the Wiener–Hopf equations are obtained, as shown here:

$$\begin{aligned}e^{-i\lambda}\Phi_-'(\lambda)-\frac{q}{\lambda+p}(e^{i(\lambda+p)}-e^{-i(\lambda+p)})+e^{i\lambda}\Phi_+'(\lambda)\\ =-\gamma(\lambda)e^{\pm i\lambda}\Phi_\mp^d(\lambda)\end{aligned} \tag{13}$$

In Eq. (13), there are two equations, whereas the number of unknowns (written in capital Greek letters) is four. This insufficient number of equations compared with the number of unknown functions can be offset by the decomposition technique at the heart of the Wiener–Hopf technique, described as follows in Sec. III.B.

B. Summary of Integral Equation Formulation

Each term in Eq. (13) can be decomposed by plus and minus functions using decomposition techniques. Multiplication decomposition is simply performed by using $\gamma(\lambda)=\gamma_-(\lambda)\gamma_+(\lambda)$. Moreover, for the summation decomposition of the terms containing the unknowns, Cauchy's integral formula was used. After placing every plus function on the left side and every minus function on the right side, and using the Abelian theorem and Liouville's theorem, four equations with four unknowns are obtained. Then, by choosing two of these equations along with the decoupling technique proposed by Noble [14], it is possible to construct two single integral equations with two unknowns, as follows:

$$\begin{aligned}\Psi_+^{1,2}(\lambda)\pm\frac{\gamma_+(\lambda)}{2\pi}\int_{-\infty+ic}^{\infty+ic}\frac{\Psi_+^{1,2}(\alpha)}{\gamma_-(\alpha)}\frac{e^{2i\alpha}}{\alpha+\lambda}\,d\alpha\\ =\gamma_+(\lambda)[F_a(\lambda)+G_a(\lambda)\pm F_b(\lambda)\pm G_b(\lambda)]\end{aligned} \tag{14}$$

where

$$\Psi_+^{1,2}(\lambda)=\Phi_+'(\lambda)\pm\Phi_-'(-\lambda)$$

$$F_{a,b}(\lambda)=\frac{qe^{\pm ip}}{\lambda\pm p}\left(\frac{1}{\gamma_+(\lambda)}-\frac{1}{\gamma_+(\mp p)}\right)$$

$$G_{a,b}(\lambda)=-\frac{qe^{\mp ip}}{\lambda\pm p}[W_0(\lambda)-W_0(\mp p)]$$

and

$$-\kappa_2\cos\theta_e<-c<\mathrm{Im}(\lambda)<c<\kappa_2\cos\theta_e$$

$$W_0(\lambda)=2e^{-2i\lambda}\frac{F_c[2\sqrt{(\kappa+\lambda)/\pi}]}{\sqrt{\kappa+\lambda}}$$

and

$$F_c(v) = 2^{-1/2} e^{-i\pi/4} \int_v^\infty e^{i\pi t^2/2}\, \mathrm{d}t$$

Here, the integral in $F_c(v)$ is the complementary Fresnel integral. Similar mathematical details are presented in Noble's work ([14], pp. 196–207).

IV. Solution in Complex Domain

A. Higher-Order Solution Technique

In this section, an improved solution technique using a Taylor series expansion of the unknown function is described. This is a generalization of the approach by Noble [14] and Kobayashi [23] who obtained a zeroth-order approximate solution. As the plus function is analytic along the given path of integration, the unknown function can be expanded by a Taylor series centered at $\alpha = \alpha_0$:

$$\Psi_+^{1,2}(\alpha) = \lim_{N\to\infty} \sum_{n=0}^{N} \frac{d^n \Psi_+^{1,2}(\alpha_0)}{n! d\alpha^n} (\alpha - \alpha_0)^n \tag{15}$$

Using a binomial expansion and deformation of the integral path along the branch cut, the integral term in Eq. (14) can be evaluated exactly, as shown next. (Note that Noble [14] and Kobayashi [23] considered the case of $N = 0$.) Details of this process are explained in a thesis by the first author [25]:

$$\int_{-\infty+ic}^{\infty+ic} \frac{\Psi_+^{1,2}(\alpha)}{\gamma_-(\alpha)} \frac{e^{2i\alpha}}{\alpha+\lambda}\, \mathrm{d}\alpha = \lim_{N\to\infty} \sum_{n=0}^{N} \frac{d^n \Psi_+^{1,2}(\alpha_0)}{n! d\alpha^n} (\kappa - \alpha_0)^n \left[\sum_{l=0}^{n} {}_nC_l \left(\frac{i}{2(\kappa-\alpha_0)} \right)^l W_l(\lambda) \right] \tag{16}$$

where

$$W_l(\lambda) = \frac{\sqrt{2}}{\pi} e^{i(2\kappa - \pi/4)} \Gamma_1\left(l + \frac{1}{2}, -2i(\kappa+\lambda) \right)$$

and

$$\Gamma_m(u,z) = \int_0^\infty \frac{t^{u-1} e^{-t}}{(t+z)^m}\, \mathrm{d}t$$

Here, ${}_nC_l$ is the binomial coefficient and $\Gamma_m(u,z)$ is the generalized gamma function defined by Kobayashi [26], which is a generalized expression of the gamma function corresponding to $m = 0$. It is important to note that the argument u has the specific form of a "nonnegative integer $+\frac{1}{2}$". Here, by putting Eq. (16) into Eq. (14), the following algebraic equations are obtained (with $\lim_{N\to\infty}$ omitted henceforth):

$$\Psi_+^{1,2}(\lambda) = \mp \sum_{n=0}^{N} \frac{d^n \Psi_+^{1,2}(\alpha_0)}{n! d\alpha^n} \left[\sum_{m=0}^{n} {}_nC_m \left(\frac{i}{2} \right)^m (\kappa - \alpha_0)^{n-m} V_m(\lambda) \right] + S^{1,2}(\lambda) \tag{17}$$

where $V_n(\lambda) = \gamma_+(\lambda) W_n(\lambda)$ and $S^{1,2}(\lambda) = \gamma_+(\lambda)[F_a(\lambda) + G_a(\lambda) \pm F_b(\lambda) \pm G_b(\lambda)]$.

By setting α_0 as κ, the complexity due to two summation symbols about n and m can be reduced using one summation symbol only about n, as follows:

$$\Psi_+^{1,2}(\lambda) = \mp \sum_{n=0}^{N} \left(\frac{i}{2} \right)^n \frac{d^n \Psi_+^{1,2}(\kappa)}{n! d\alpha^n} V_n(\lambda) + S^{1,2}(\lambda) \tag{18}$$

Differentiating both sides of Eq. (18) with respect to λ by m times (for $m = 0 \sim N$) and putting κ into λ allows the construction of $N+1$ simultaneous algebraic equations to determine $N+1$ unknown differential coefficients in the summation symbol:

$$\frac{d^m}{d\lambda^m} \Psi_+^{1,2}(\kappa) \pm \sum_{n=0}^{N} \left(\frac{i}{2} \right)^n \frac{1}{n!} \frac{d^m}{d\lambda^m} V_n(\kappa) \frac{d^n}{d\lambda^n} \Psi_+^{1,2}(\kappa) = \frac{d^m}{d\lambda^m} S^{1,2}(\kappa) \quad \text{for } m = 0 \sim N \tag{19}$$

These equations can be rewritten in matrix form by Eq. (20), where the matrix $\mathbf{A}^{1,2}$ and vectors $\mathbf{X}^{1,2}$ and $\mathbf{B}^{1,2}$ are given as

$$\mathbf{A}^{1,2} \mathbf{X}^{1,2} = \mathbf{B}^{1,2} \tag{20}$$

where

$$\mathbf{A}^{1,2} = [a_{mn}^{1,2}]_{(N+1)(N+1)}, \quad \mathbf{X}^{1,2} = [x_m^{1,2}]_{N+1}, \quad \text{and} \quad \mathbf{B}^{1,2} = [b_m^{1,2}]_{N+1}$$

and where

$$a_{mn}^{1,2} = \delta_{mn} \pm \left(\frac{i}{2} \right)^n \frac{1}{n!} \frac{d^m}{d\lambda^m} V_n(\kappa)$$

$$x_m^{1,2} = \frac{d^m}{d\lambda^m} \Psi_+^{1,2}(\kappa)$$

$$b_m^{1,2} = \frac{d^m}{d\lambda^m} S^{1,2}(\kappa)$$

and δ_{mn} is the Kronecker delta.

By solving Eq. (20), the differential coefficients are evaluated. Thus, the solution is completed in series form by Eq. (18). Simply by increasing the number of terms, a more accurate higher-order series solution is obtained. For the evaluation of the matrix, whose entries contain the generalized gamma function and its derivatives, the exact and closed-form formula of the generalized gamma function suitable for this problem is used, as the original function is in integral form.

B. Exact Formulas of Generalized Gamma Functions and Complex Potential

Upon the first appearance of the generalized gamma function in Kobayashi's [26] paper (cf. Noble's [14] used the notation of the Whittaker function, suitable for his asymptotic zeroth-order analysis, which corresponds to $m = 1$ in the generalized gamma function $\Gamma_m(u,z)$), the importance of this special function was emphasized, especially with respect to the mathematical theory of diffraction related to the Wiener–Hopf technique. Kobayashi also investigated a number of mathematical properties, formulas, and recurrence relations of this special function. Several papers dealing with this special function have been reported in recent years; notably, Srivastava et al. [27] summarized and unified the previous mathematical expressions. In the present paper, the exact and closed-form formula of the generalized gamma function, which is useful for the proposed finite diffraction problem, is introduced for the specific argument of $u =$ positive integer $+\frac{1}{2}$. As the derivation procedures and the mathematical details can be found in an earlier paper by the authors [24], only the results are introduced here.

Equation (21) shows the exact formula of the generalized gamma function for a real argument z. Here, $\Gamma(z)$ is the well-known gamma function corresponding to $m = 0$ and "erfc" is a complementary error function:

$$\Gamma_1(n+1/2, z) = \sum_{k=0}^{n-1} (-z)^{n-1-k} \Gamma(k+1/2) + (-)^n \pi \lambda^{n-1/2} e^{\lambda} \mathrm{erfc}(\sqrt{\lambda}) \tag{21}$$

For a suitable form for the proposed problem, putting $-2i(\kappa+\lambda)$ into z, Eq. (21) is rewritten as Eq. (22):

$$\Gamma_1(n+1/2,-2i(\kappa+\lambda)) = \sum_{k=0}^{n-1}[2i(\kappa+\lambda)]^{n-1-k}\Gamma(k+1/2) + (-)^n 2\pi[-2i(\kappa+\lambda)]^{n-1/2}e^{-2i(\kappa+\lambda)}F_c[\sqrt{2(\kappa+\lambda)/\pi}] \quad (22)$$

As shown in Eq. (22), the generalized gamma function occurring in the finite diffraction theory is expressed by a combination of the Fresnel integral and polynomials. The role of the Fresnel integral in diffraction theory is apparent, not only in semi-infinite diffraction but also in the finite diffraction phenomena. The formula for the arbitrary positive integer m is also obtained using Eq. (23), by simply differentiating Eq. (22) $(m-1)$ times with respect to λ:

$$\Gamma_m(n+1/2,-2i(\kappa+\lambda)) = \frac{(2i)^{-m+1}}{(m-1)!}\frac{d^{m-1}}{d\lambda^{m-1}}\left[\sum_{k=0}^{n-1}[2i(\kappa+\lambda)]^{n-1-k}\Gamma(k+1/2) + (-)^n 2\pi[-2i(\kappa+\lambda)]^{n-1/2}e^{-2i(\kappa+\lambda)}F_c\left(2\sqrt{\frac{\kappa+\lambda}{\pi}}\right)\right] \quad (23)$$

Finally, by solving Eq. (20) using the formula of Eq. (23), a complete series solution for the transformed potential in complex domain is obtained, as follows:

$$\Phi(\lambda,\eta) = \begin{cases} A(\lambda)e^{-\gamma(\lambda)\eta}, & \eta \geq 0 \\ -A(\lambda)e^{\gamma(\lambda)\eta}, & \eta \leq 0 \end{cases} \quad (24)$$

where

$$A(\lambda) = -\gamma^{-1}(\lambda)[e^{-i\lambda}\Phi'_-(\lambda,0) + \Phi'_0(\lambda,0) + e^{i\lambda}\Phi'_+(\lambda,0)] = A_1(\lambda) + A_2(\lambda) + A_3(\lambda)$$

where

$$A_1(\lambda) = -\frac{iqe^{-i(\lambda+p)}}{(\lambda+p)\sqrt{\kappa+\lambda}\sqrt{\kappa+p}},$$

$$A_2(\lambda) = \frac{iqe^{i(\lambda+p)}}{(\lambda+p)\sqrt{\kappa-\lambda}\sqrt{\kappa-p}}$$

and

$$A_3(\lambda) = -\frac{ie^{i\lambda}}{\sqrt{\kappa-\lambda}}\left(G_a(\lambda) - \sum_{n=0}^{N}\left(\frac{i}{2}\right)^n\frac{1}{n!}\frac{x_n^1 - x_n^2}{2}W_n(\lambda)\right) - \frac{ie^{-i\lambda}}{\sqrt{\kappa+\lambda}}\left(G_b(-\lambda) - \sum_{n=0}^{N}\left(\frac{i}{2}\right)^n\frac{1}{n!}\frac{x_n^1 + x_n^2}{2}W_n(-\lambda)\right)$$

This series solution is the first solution obtained without using separable coordinates, such as the elliptic cylinder coordinates that yielded an exact solution of the Mathieu series. The series solution can provide more accurate results simply by solving the linear algebraic equation [i.e., Eq. (20)] in an arbitrary higher order, thereby assuring convergence. To check the convergence of this series solution, the authors investigated the convergence property of this series solution in the complex domain before performing inverse Fourier transforms. As one measure of convergence, the real part of $A(\lambda)$ along the path of integration for the inverse Fourier transform was examined by increasing N. As the imaginary part of the path of integration is infinitesimally small, the imaginary part is considered as one-hundredth of its real part. It is then possible to check the converging behavior of the present series solution. This series solution showed fast convergence at a high-frequency region, so that only a small number of terms were required to complete the convergence. As the frequency was lowered, additional terms were necessary for convergence (cf. N was 1 for $\kappa = 10$, N was 2 for $\kappa = 5$, and N was 4 for $\kappa = 1$). This convergence behavior contrasts with that of the Mathieu series, which shows faster convergence at a lower frequency rather than at a higher frequency.

V. Solution in Physical Domain: Visualizations and Interpretations

A. Exact and Asymptotic Inverse Fourier Transforms of Complex Potential

The first term in complex potentials referring to A_1 in Eq. (24) is exactly evaluated by deforming the original path of integration into a hyperbola and a large circular arc connecting the original path, as follows:

$$\phi_1^u(r_1,\theta_1) = e^{-ik\cos\theta_e}\{I_0(r_1,-\theta_1+\theta_e) - I_0(r_1,-\theta_1-\theta_e) - e^{ikr_1\cos(\theta-\theta_e)}[1+\mathrm{sgn}(\theta_e-\theta_1)]/2\} \quad (25a)$$

$$\phi_1^l(r_1,\theta_1) = -e^{-ik\cos\theta_e}\{I_0(\alpha=-\theta_1+\theta_e) - I_0(\alpha=-\theta_1-\theta_e) - e^{ikr_1\cos(\theta+\theta_e)}[1+\mathrm{sgn}(\theta_e+\theta_1)]/2\} \quad (25b)$$

where

$$I_0(r,\theta) = \mathrm{sgn}[\sin(\theta/2)]e^{ikr\cos\theta}F_c(2\sqrt{kr/\pi}|\sin(\theta/2)|)$$

and

$$F_c(v) = 2^{-1/2}e^{-i\pi/4}\int_v^\infty e^{it^2\pi/2}\,dt$$

Here, the superscripts u and l indicate regions of the upper half $(0<\theta_1<\pi)$ and the lower half $(-\pi<\theta_1<0)$ in the physical plane, respectively, and the polar coordinates are defined by $\xi+1 = r_1\cos\theta_1$, $\eta = r_1\cos\theta_1$, where $-\pi<\theta_1<\pi$.

Likewise, the exact evaluation of the second term referring to A_2 can be obtained as follows:

$$\phi_2^u(r_2,\theta_2) = e^{ik\cos\theta_e}\{I_0(\alpha=\theta_2-\theta_e) + I_0(\alpha=\theta_2+\theta_e) + e^{ikr_2\cos(\theta_2-\theta_e)}[1+\mathrm{sgn}(\theta_e-\theta_2)]/2\} \quad (26a)$$

$$\phi_2^l(r_2,\theta_2) = -e^{ik\cos\theta_e}\{I(\alpha=-\theta_2-\theta_e) + I(\alpha=-\theta_2+\theta_e) + e^{ikr_2\cos(\theta_2+\theta_e)}[1+\mathrm{sgn}(\theta_e+\theta_2)]/2\} \quad (26b)$$

In this formula, the polar coordinates are defined by $\xi-1 = r_2\cos\theta_2$, $\eta = r_2\cos\theta_2$, where $-\pi<\theta_1<\pi$.

For the third term referring to A_3 in Eq. (24), there is no direct method to evaluate the integral exactly. Therefore, the method of steepest descent was applied. Hence, the asymptotic result is given as

$$\phi_3(r,\theta) \approx \sqrt{k/2\pi r}e^{i(kr-\pi/4)}\sin\theta\, A_3(-k\cos\theta) \quad (27)$$

Apparently, Eq. (27) has a couple of singular points when the observation angle θ coincides with the incidence angle of $\theta=\theta_e$, the reflection angle of $\theta=-\theta_e$, $\theta=\pi$, and $\theta=0$. However, as all singular points are removable singularities, no singular problem appears.

B. Visualization and Interpretation of the First Term

First, it is not difficult to recognize that ϕ_1 in Eqs. (25a) and (25b) is identical to the solution of diffraction by a semi-infinite strip $(-1<x<\infty,\ y=0)$; this is clearly shown in Figs. 2a and 2b. Figure 2a shows the total acoustic field by adding the incident plane wave for $\theta_i = \pi/4$ and $kl = 10$. Here, the physical domain is divided roughly into three regions: 1) a zone of shadow $(0<\theta_1<\theta_i)$, 2) a zone of illumination $(\theta_i<|\theta_1|<\pi)$, and 3) a zone of reflection $(-\theta_i<\theta_1<0)$. Figure 2b shows only the scattered acoustic field. The *minus* incident wave exists in the zone of shadow, because this region is behind the semi-infinite strip. In the zone of illumination, spherically propagating diffracted waves emitted from the sharp leading edge can be observed clearly, and in the zone of reflection, there is a *plus* reflection wave.

Now, to show the effect of fluid convection, the solution in the NPG coordinates is converted into the physical domain, as shown in Fig. 3 for $M = 0.5$. Here, the illuminated region is extended to the

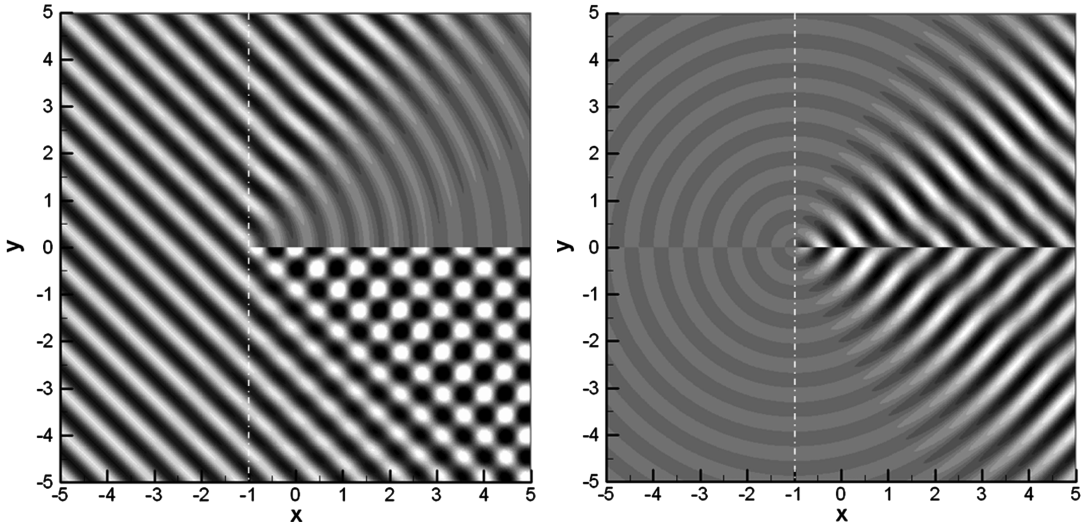

Fig. 2 Acoustic field for $kl = 10$ and $\theta_i = \pi/4$: a) $\mathrm{Re}(\phi_1 + \phi_i)$, b) $\mathrm{Re}(\phi_1)$.

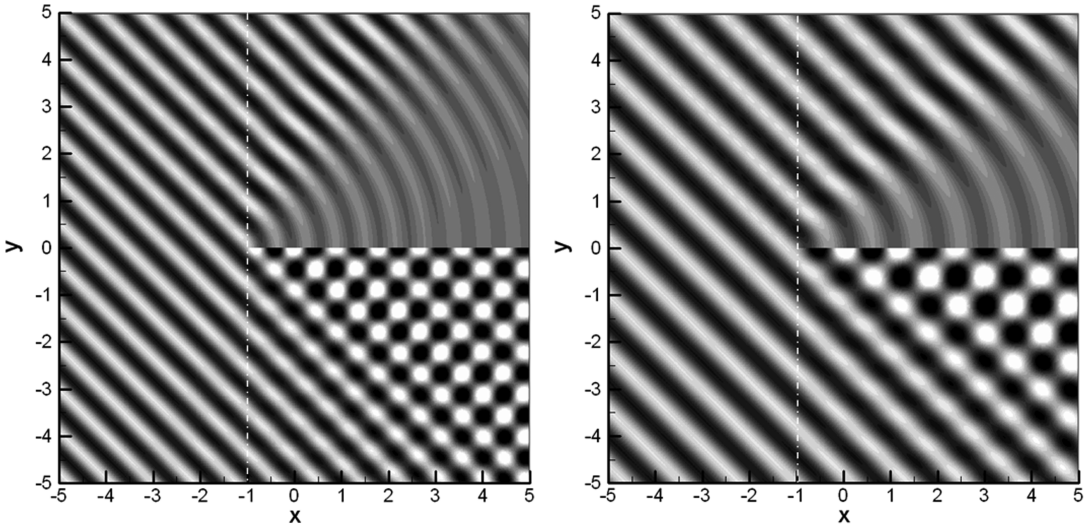

Fig. 3 Effect of fluid convection for $kl = 10$ and $\theta_i = \pi/4$: a) $M = 0$, b) $M = 0.5$.

shadow zone due to the uniform flow, and the wavelength and the speed of propagation are increased, as shown in Fig. 3b. In addition, as the direction of the wave and the flow are identical, the amplitude is decreased due to extension of the wave.

C. Visualization and Interpretation of the Second Term

In this section, the second term referring to ϕ_2 in Eqs. (26a) and (26b) is visualized and interpreted with its physical meaning. Figure 4a shows the total acoustic field of $\phi_1 + \phi_2 + \phi_i$ for $\theta_i = \pi/4$ and $kl = 10$. Here, the zone of shadow is observed, where diffracted waves by leading and trailing edges are superposed behind the finite strip. In the zone of reflection, checked patterns superposed by the incident and reflected waves can be seen clearly.

In Fig. 4b, minus incident waves and reflected waves are observed in the zone of shadow and zone of reflection, respectively. Additionally, in the zone of illumination, distorted spherical waves that are emitted from the sharp leading and trailing edges can be observed. In Sec. V.B, the first term indicates scattering by a semi-infinite leading edge. By adding this second term, geometrical finiteness is roughly considered; therefore, the second term plays a role of trailing-edge correction to the first term. Further physical meaning of the second term is considered heuristically in Sec. V.E.

D. Visualization and Interpretation of the Third Term

Lastly, the physical meaning of the third term referring to ϕ_3 in Eq. (27) was investigated. As the contour plots of the total and scattered acoustic fields including ϕ_3 are similar to what is shown in Fig. 4, the directivity pattern is plotted for a quantitative comparison. Figure 5 shows the directivity of a scattered wave normalized by an incident wave. The dashed and solid lines indicate the solution of $\phi_1 + \phi_2$ and $\phi_1 + \phi_2 + \phi_3$, respectively. In Fig. 5a, for $kl = 10$ and $\theta_i = \pi/4$, we can observe that the difference between the dashed and solid lines is very small, except for the region of $\theta = 0$ and $\theta = \pi$. (The solid line represents the converged solution of $N = 1$, and this convergence was checked in the manner explained at the end of Sec. IV.B.) However, in Fig. 5b, for $kl = 5$ and $\theta_i = \pi/4$, the difference between the dashed and solid lines is clearly seen everywhere, unlike in Fig. 5a. In the case of the low frequency $kl = 5$, the converged solution was obtained for $N = 2$. Furthermore, for a lower value of kl, the number of N for convergence increases.

This indicates that the contribution of the higher-order terms in the present series solution increases as the incident frequency decreases. In other words, the interaction between the leading and trailing edges is more important for intermediate and low frequencies, whereas it can be negligible at a high frequency. As the third term referring to ϕ_3

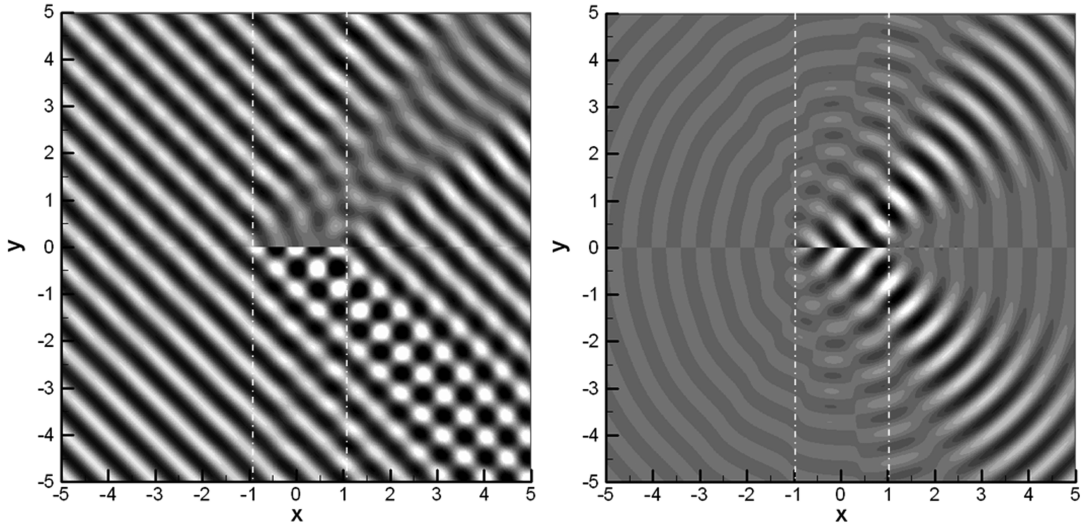

Fig. 4 Acoustic field for $kl = 10$ and $\theta_i = \pi/4$: a) $\mathrm{Re}(\phi_1 + \phi_2 + \phi_i)$, b) $\mathrm{Re}(\phi_1 + \phi_2)$.

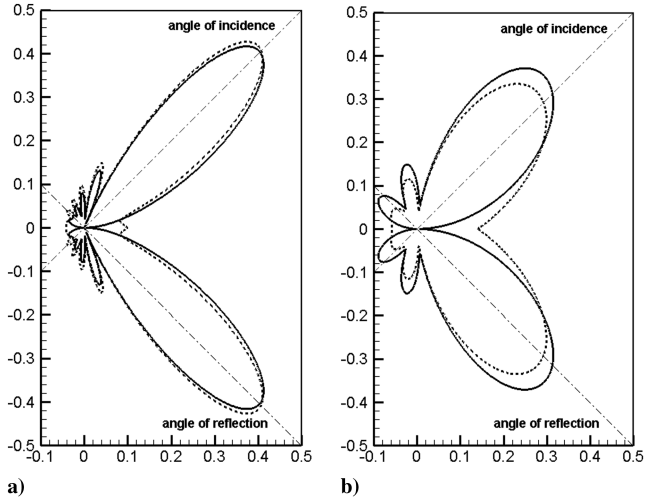

Fig. 5 Directivity patterns of $\phi_1 + \phi_2$ (dashed) and $\phi_1 + \phi_2 + \phi_3$ (solid): a) $kl = 10$, b) $kl = 5$.

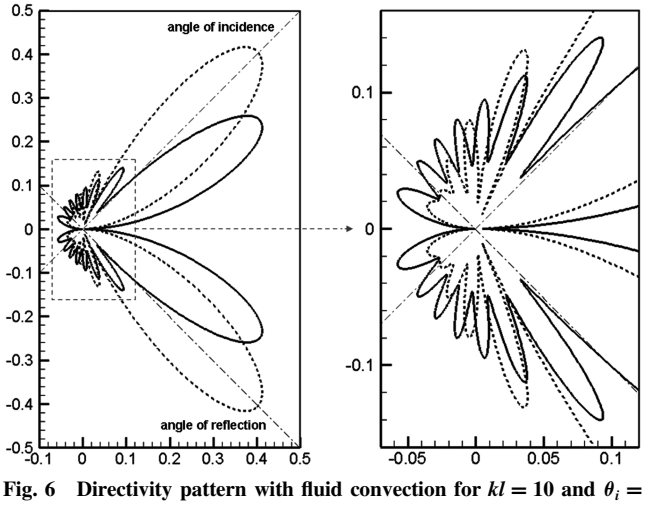

Fig. 6 Directivity pattern with fluid convection for $kl = 10$ and $\theta_i = \pi/4$ (dashed line: $M = 0$, solid line: $M = 0.5$).

played the role of eliminating the discrepancies around the leading ($\theta = \pi$) and trailing ($\theta = 0$) edges, this term can be interpreted by the interaction between these edges.

To observe the effect of fluid convection for the finite diffraction phenomena, the directivity pattern in the presence of a uniform flow is compared for $M = 0$ and $M = 0.5$ in Fig. 6. This figure shows the effect of fluid convection such that the lobe is inclined along the flow direction, and the magnitude of the downstream wave decreases due to the extension of the wave that stems from the identical directions of the wave and the flow.

Meanwhile, the amplitude and the wave number of the diffracted wave propagating upstream are increased due to the compression of the wave, as the flow direction is the opposite of the wave direction.

E. Further Investigation of the Second Term: A Heuristic Description

In the preceding section, the physical meaning of the second term referring to ϕ_2 is given roughly by a trailing-edge correction. In this section, the geometric finiteness is heuristically examined and an interesting meaning of the second term is found. For this supplementary investigation, the total acoustic fields by a single leading edge at $x = -1$ and a single trailing edge at $x = 1$ are demonstrated, respectively.

First, the total acoustic field by a single leading edge is shown in Fig. 7 for $kl = 10$ and $\theta_i = \pi/4$. Figure 7a shows the schematics of the acoustic field in the sense of geometric decomposition. Here, dL indicates the diffracted wave by the leading edge, and i and r indicate the incident and reflected waves, respectively.

The waves in the zone of shadow, in the zone of illumination, and in the zone of reflection are clearly seen in Fig. 7b as decomposed in Fig. 7a. Likewise, the total acoustic field by a single trailing edge at $x = 1$ can be decomposed, as shown in Fig. 8a. Similarly, dT indicates the diffracted wave by the trailing edge, and i and r indicate the incident and reflected waves, respectively. Figure 8b shows the real acoustic field, which is in approximate agreement with the geometric decomposition presented in Fig. 8a.

Now, Figs. 7b and 8b are superposed and the meaning of this superposition is illustrated in Fig. 9. If dL were continuous across the semi-infinite leading edge and dT were continuous across the semi-infinite trailing edge, the only difference between the upper- and lower-half plane across $y = 0$ would be $i + r$, as shown in Fig. 9a. This indicates that, if the redundant "incident + reflected" waves in the lower-half plane were removed, the approximate acoustic field by a finite strip could be obtained, not by solving a complicated three-part mixed boundary value problem, but by solving two semi-infinite problems involving two-part mixed boundary conditions. The superposed acoustic field and redundant-wave-removed field are shown in Figs. 9b and 10b.

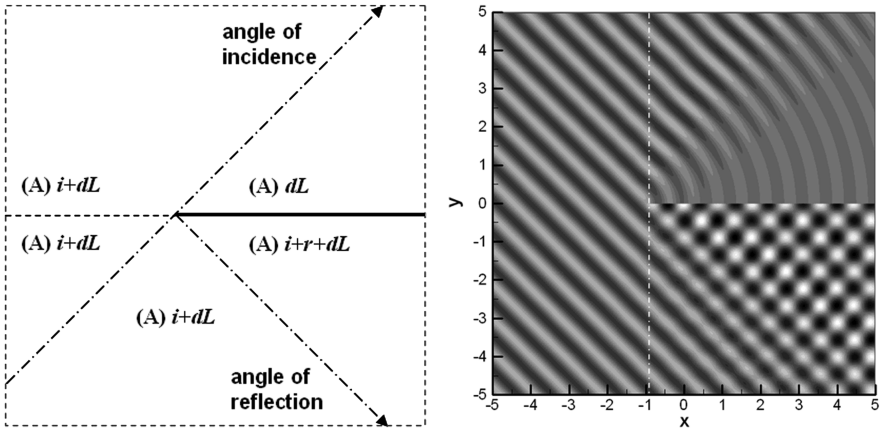

a) b)

Fig. 7 Scattering by a semi-infinite leading edge at $x = -1$ ($kl = 10$, $\theta_i = \pi/4$): a) schematics, b) total acoustic field.

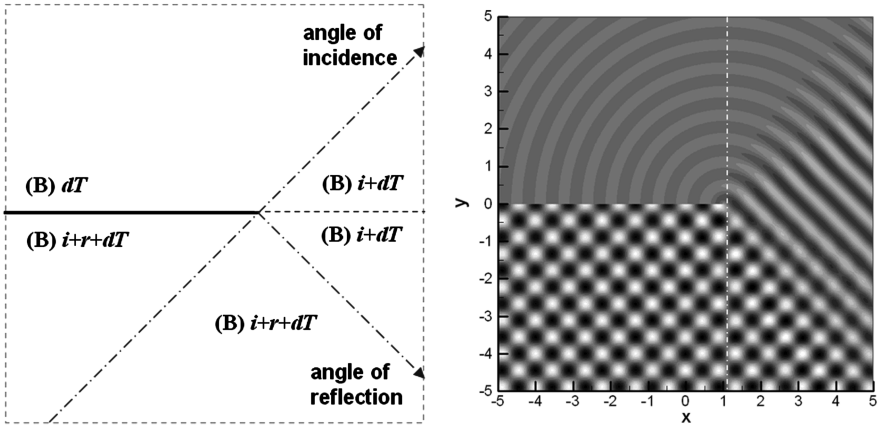

a) b)

Fig. 8 Scattering by a semi-infinite trailing edge at $x = 1$ ($kl = 10$, $\theta_i = \pi/4$): a) schematics, b) total acoustic field.

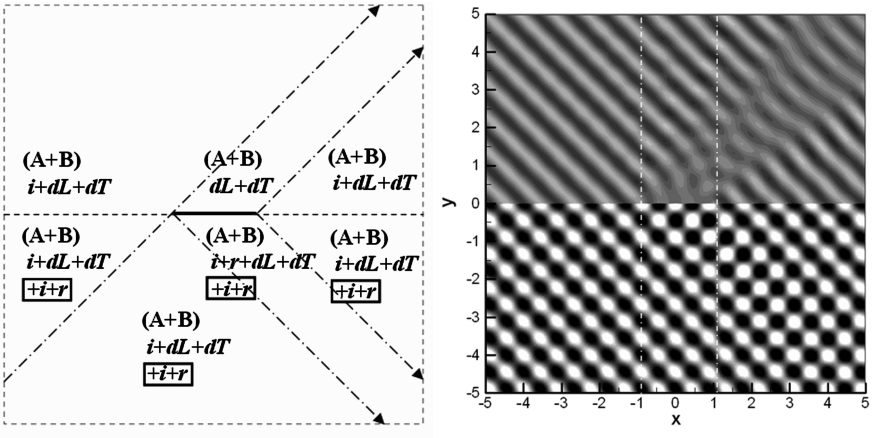

a) b)

Fig. 9 Superposition of the leading and trailing edges ($kl = 10$, $\theta_i = \pi/4$): a) schematics, b) acoustic field.

Clearly, as dL behind the trailing edge and dT ahead of the leading edge are not continuous across $y = 0$, this geometric consideration cannot provide a correct result for finite diffraction. However, by virtue of this consideration, an interesting physical meaning of the second term was found in the analytic solution by plotting the directivity of the scattered acoustic field at $R = 10l$. Figure 11a shows the directivity pattern of the heuristically constructed acoustic field. Surprisingly, the directivity of this heuristic description is identical to the directivity pattern of $\phi_1 + \phi_2$, as shown in Fig. 11b.

This signifies that ϕ_2 provides 1) an addition of a semi-infinite trailing-edge solution and 2) the removal of the redundant field of "incident" and "reflected" waves in the lower-half plane. This heuristic description of geometric finiteness represents the physical meaning of the mathematical formula of ϕ_2.

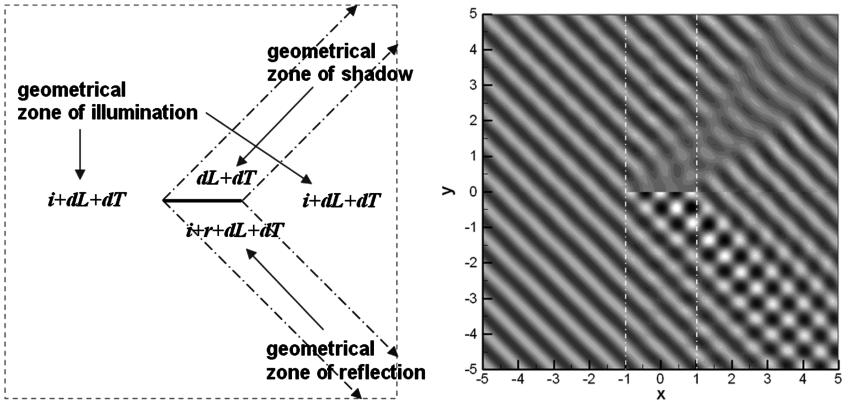

a) b)

Fig. 10 Removal of the redundancy ($kl = 10, \theta_i = \pi/4$): a) schematics, b) acoustic field.

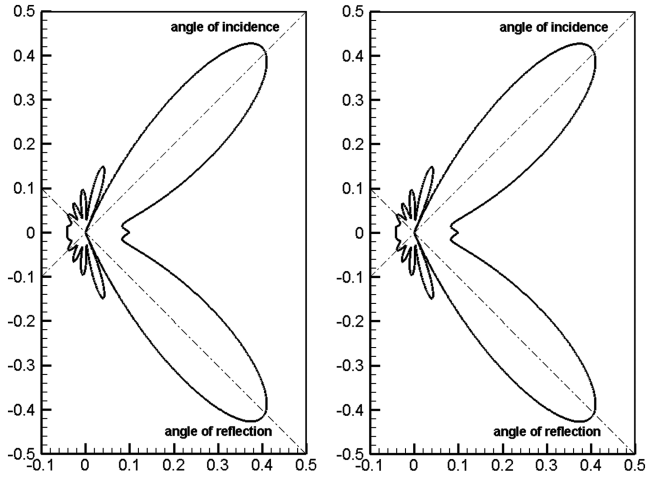

a) b)

Fig. 11 Directivity pattern ($kl = 10, \theta_i = \pi/4$): a) heuristically decomposed solution, b) $\phi_1 + \phi_2$.

If the frequency of the incident wave is high enough that the geometric decomposition of acoustic field is reasonable, the finite diffraction phenomena can be roughly replaced by this heuristic description with reasonable accuracy except for the leading- ($\theta = \pi$) and trailing- ($\theta = 0$) edge regions, as shown in Fig. 5a.

VI. Conclusions

As a fundamental study of aerodynamic sound diffraction by a thin airfoil, an advanced mathematical analysis of the Wiener–Hopf integral equation was presented. Whereas the integral equation approaches performed by Noble [14] and Kobayashi [23] were restricted to a zeroth-order approximate solution, in this paper, the authors improved the accuracy of the solution by expanding the unknown inside the integral by a Taylor series in an arbitrary order. By evaluating each term of the integrand analytically, the original integral equations with a multivalued kernel could be recast into simultaneous algebraic equations of the unknown differential coefficients of the Taylor series. The exact and closed-form formulas of the generalized gamma function derived by the authors played an important role in the evaluation of the matrix entries and thus in the acquisition of the complete series solution. The convergence of the series solution was investigated in the physical domain and in the complex domain. The present series solution shows faster convergence in the high-frequency range relative to the low-frequency range, which is the opposite property of the Mathieu series solution. The second-half of the paper is devoted to visualizing and interpreting the diffracted acoustic fields. By virtue of the visualizations, it was possible to observe the multiple-edge diffraction phenomena in the presence of fluid convection and to understand the physical meaning of the complicated mathematical solution. It is hoped that the present analytic solution will contribute to the development of computational aeroacoustics in the numerical treatment of sharp edges and inflow/outflow boundary conditions.

References

[1] Sommerfeld, A., "Mathematische Theorie der Diffraction," *Mathematische Annalen*, Vol. 47, Nos. 2–3, 1896, pp. 317–374. doi:10.1007/BF01447273

[2] Schwarzschild, K., "Die Beugung und Polarisation des Lichts durch einen Spalt. I," *Mathematische Annalen*, Vol. 55, No. 2, 1901, pp. 177–247. doi:10.1007/BF01444971

[3] Amiet, R. K., "High Frequency Thin Airfoil Theory for Subsonic Flow," *AZAA Journal*, Vol. 14, No. 8, 1976, pp. 1076–1082.

[4] Martinez, R., and Widnall, S. E., "Unified Aerodynamic-Acoustic Theory for a Thin Rectangular Wing Encountering a Gust," *AIAA Journal*, Vol. 18, No. 6, 1980, pp. 636–645. doi:10.2514/3.7675

[5] Mathieu, E., "Mémoire sur le Mouvement Vibratoire d'une Membrane de forme Elliptique," *Journal des Mathématiques Pures et Appliquées*, Vol. 13, No. 2, 1868, pp. 137–203.

[6] Morse, P. M., and Rubenstein, P. J., "The Diffraction of Waves by Ribbons and by Slits," *Physical Review*, Vol. 54, No. 11, 1938, pp. 895–898. doi:10.1103/PhysRev.54.895

[7] Sieger, B., "Die Beugung einer ebenen elektrischen Welle an einem Schirm von elliptischem Querschnitt," *Annalen der Physik*, Vol. 332, No. 13, 1908, pp. 626–664. doi:10.1002/andp.19083321306

[8] Agarwal, A., and Dowling, A. P. "The Calculation of Acoustic Shielding of Engine Noise by Silent Aircraft Airframe," *11th AIAA/CEAS Aeroacoustics Conference*, AIAA Paper 2005-2996, 2005.

[9] Frenkel, D., and Portugal, R., "Algebraic Methods to Compute Mathieu Functions," *Journal of Physics, A: Mathematical and General*, Vol. 34, No. 17, 2001, pp. 3541–3551. doi:10.1088/0305-4470/34/17/302

[10] Whitakker, E. T., "On the General Solution of Mathieu's Equation," *Proceedings of the Edinburgh Mathematical Society*, Vol. 32, Edinburgh Mathematical Society, Edinburgh, 1914, pp. 75–80.

[11] Keller, J. B., "Geometrical Theory of Diffraction," *Journal of the Optical Society of America*, Vol. 52, No. 2, 1962, pp. 116–130.

[12] Luneburg, E., "The Sommerfeld Problem: Methods, Generalizations and Frustrations," *Modern Mathematical Methods in Diffraction Theory and Its Applications in Engineering: Proceedings of the Sommerfeld '96 Workshop*, edited by M. Meister, 1996.

[13] Wiener, N., and Hopf, E., "Uber eine Klasse singularer Integralgleichungen," *Sitzungsberichte der Preussischen Akademie der Wissenschaften*, Vol. 31, 1931, pp. 696–706.

[14] Noble, B., *Methods Based on the Wiener–Hopf Technique*, Pergamon Press, Oxford, 1958.

[15] Abrahams, I. D., and Lawrie, J. B., "On the Factorization of a Class of Wiener–Hopf Kernels," *IMA Journal of Applied Mathematics*, Vol. 55,

No. 1, 1995, pp. 35–47.
doi:10.1093/imamat/55.1.35
[16] Abrahams, I. D., "The Application of Pade Approximant to Wiener–Hopf Factorization," *IMA Journal of Applied Mathematics*, Vol. 65, No. 3, 2000, pp. 257–281.
doi:10.1093/imamat/65.3.257
[17] Crighton, D. G., "Asymptotic Factorization of Wiener–Hopf Kernels," *Wave Motion*, Vol. 33, No. 1, 2001, pp. 51–65.
doi:10.1016/S0165-2125(00)00063-9
[18] Latta, G. E., "The Solution of a Class of Integral Equations," *Journal of Rational Mechanics and Analysis*, Vol. 5, No. 5, 1956, pp. 821–834.
[19] Williams, M. H., "Diffraction by a Finite Strip," *Quarterly Journal of Mechanics and Applied Mathematics*, Vol. 35, No. 1, 1982, pp. 103–124.
doi:10.1093/qjmam/35.1.103
[20] Shanin, A. V., "Three Theorems Concerning Diffraction by a Strip or a Slit," *Quarterly Journal of Mechanics and Applied Mathematics*, Vol. 54, No. 1, 2001, pp. 107–137.
doi:10.1093/qjmam/54.1.107
[21] Shanin, A. V., "A Generalization of the Separation of Variables Method for Some 2D Diffraction Problems," *Wave Motion*, Vol. 37, No. 3, 2003, pp. 241–256.
doi:10.1016/S0165-2125(02)00077-X
[22] Jones, D. S., "A Simplifying Technique in the Solution of a Class of Diffraction Problems," *Quarterly Journal of Mathematics*, Vol. 3, No. 1, 1952, pp. 189–196.
doi:10.1093/qmath/3.1.189
[23] Kobayashi, K., "Plane Wave Diffraction by a Strip: Exact and Asymptotic Solutions," *Journal of the Physical Society of Japan*, Vol. 60, No. 6, 1991, pp. 1891–1905.
doi:10.1143/JPSJ.60.1891
[24] Jeon, W., and Lee, D.-J., "Exact and Useful Formulas of Generalized Gamma Functions Occurring in Finite Diffraction Theory," *Integral Transforms and Special Functions*, Vol. 19, No. 10, 2008, pp. 735–745.
doi:10.1080/10652460802326898
[25] Jeon, W., "An Analytic Study of Acoustic Diffraction by a Finite Strip in Convected Medium," Ph.D. Dissertation, Aerospace Engineering Dept., Korea Advanced Inst. of Science and Technology, Daejeon, Republic of Korea, 2006.
[26] Kobayashi, K., "On Generalized Gamma Functions Occurring in Diffraction Theory," *Journal of the Physical Society of Japan*, Vol. 60, No. 5, 1991, pp. 1501–1512.
doi:10.1143/JPSJ.60.1501
[27] Srivastava, H. M., Saxena, R. K., and Chena Ram., "A Unified Presentation of the Gamma-Type Functions Occurring in Diffraction Theory and Associated Probability Distributions," *Applied Mathematics and Computation*, Vol. 162, No. 2, 2005, pp. 931–947.
doi:10.1016/j.amc.2003.12.133

R. So
Associate Editor